Supporting Information

Spectroscopic and Reactivity Differences in Metal Complexes Derived from Sulfur Containing Triphos Homologs

A. Petuker,[a‡] P. Gerschel,[a‡] S. Piontek,[a‡] N. Ritterskamp,[a] F. Wittkamp,[a] L. Iffland,[a] R. Miller,[a] M. van Gastel[b] and U.-P. Apfel[a*]

[a] Ruhr University Bochum, Inorganic Chemistry I, Universitätsstraße 150, 44801 Bochum.

[b] Max-Planck-Institut für Chemische Energiekonversion, Stiftstraße 34-36, 45470 Mülheim

‡ These authors contributed equally.

Content

Experimental Section 3

Electrochemistry. 3

Spectroelectrochemistry 3

X-ray Data Collection and Structure Solution Refinement 3

Density Functional Theory Calculations 4

Figure S1 UV/vis spectra of **7** and **8** 5

Figure S2 SEC-IR of **11** in THF 5

Figure S3 SEC-IR of **11** in MeCN 6

Figure S4 SEC-IR of **12** in MeCN 6

Figure S5 SEC-IR of **13** in THF 7

Figure S6 SEC-IR of **13** in MeCN 7

Figure S7 SEC-IR of **14** in THF 8

Table S1 Calculated Gibbs free energies of Mo^0-complexes 9

Table S2 Calculated Gibbs free energies of Mo^I-complexes 9

Table S3 General overview of binding mode changes in MeCN 9

Figure S8 GC of catalysis + **SSS** 10

Figure S9 GC of catalysis + **PSS** 10

Figure S10 GC of catalysis + **PPS** 11

Figure S11 GC of catalysis + **PPP** 11

Table S4 Crystal Data and Refinment 12

References 14

Experimental Section

Electrochemistry. Cyclic and linear sweep voltammetry of the complexes was performed on a GAMRY Reference 600 or a PalmSens3 potentiostat using a standard three-electrode setup. A glassy carbon (GC) electrode was used as working electrode, a Ag wire as quasi-reference and a Pt wire as counter electrode. In electrochemical experiments, either in anhydrous MeCN or anhydrous THF, 0.1 M tetrabutylammonium hexafluorophosphate ($TBAPF_6$) was used as electrolyte. Prior to each experiment, the electrochemical cell was degassed for at least 10 min by using argon, and an argon atmosphere was maintained throughout the measurements. The GC working electrode was prepared by successive polishing with 1.0 and 0.3 μm alumina pastes and sonicated in MeCN for 5 min. All cyclic voltammograms were recorded at a scan rate of 100 mV/s and measured potentials were referenced to the ferrocene/ferrocenium couple (Fc/Fc^+).

Spectroelectrochemistry. IR-SEC measurements were carried out on a SP-02 cell (*Spectroelectrochemistry Partners*) attached to a Bruker Tensor 27 FT-IR spectrometer with a *Pike* Miracle ATR unit. A PalmSens3 was used as potentiostat with a standard three-electrode setup. The electrodes in the IR-SEC cell consist of a glassy carbon (GC) electrode as the working electrode, a Ag wire as quasi-reference and a Pt wire as counter electrode. All measurements were carried out in solutions containing 20 mM of the Mo^0 species and 0.1 M $TBAPF_6$. Prior to each experiment, the electrochemical cell was degassed for at least 10 min by using argon, and kept under an argon atmosphere throughout the measurements. The GC working electrode was prepared by successive polishing with 1.0 and 0.3 μm alumina pastes and sonicated in MeCN, respectively THF for 5 min. The GC electrode was placed 200 μm above the ATR crystal and the potential was held for 400 s before the IR scan was initiated. The scans (128 scans) were completed in roughly 260 s.

X-ray Data Collection and Structure Solution Refinement. Single crystals suitable for X-ray structure analysis were coated with Paratone N oil, mounted on a fiber loop, and placed in a cold, gaseous dinitrogen stream on the diffractometer. For **9** Rigaku XtaLABmini diffractometer performing ω scans at 293 K was used. Diffraction intensities were measured using graphite-monochromatic Mo Kα radiation (λ = 0.71075 Å). For **12**, **14** Oxford XCalibur diffractometer performing φ and ω scans at 170(2) K. Diffraction intensities were measured using graphite-monochromatic Mo Kα

radiation (λ = 0.71073 Å). For **8**, **11**, **13** SuperNova diffractometer performing φ and ω scans at 120(2) K. Diffraction intensities were measured using graphite-monochromatic Cu Kα radiation (λ = 1.54184 Å). Data collection, indexing, initial cell refinements, frame integration, final cell refinements, and absorption corrections were accomplished with the program CrysAlisPro,[1] Space groups were assigned by analysis of the metric symmetry and systematic absences (determined by XPREP or WinGX[2]) and were further checked by PLATON[3,4] for additional symmetry. Structures were solved by direct methods and refined against all data in the reported 2θ ranges by full-matrix least squares on F^2 with the SHELXL program suite[5] using the OLEX2 or shelXle interface.[6,7] Crystallographic data as well as refinement parameters are presented in Table S4. **14** was solved using `SIMU` and `DELU` restraints on carbon atoms and the `EADP` constraint for the carbon and oxygen atoms of the positional disordered CO moiety. In case of **11**, a disordered THF molecule located at the inversion center is present in the molecular structure.

Density Functional Theory Calculations. DFT calculations were performed with the ORCA program package.[8] Geometry optimization *in vacuo* and geometry optimization was carried out with the BP86 functional[9] and a polarized triple-zeta basis set (Def2-TZVP).[10] Scalar relativistic corrections are included within the zero-th order regular approach (ZORA).[11,12]

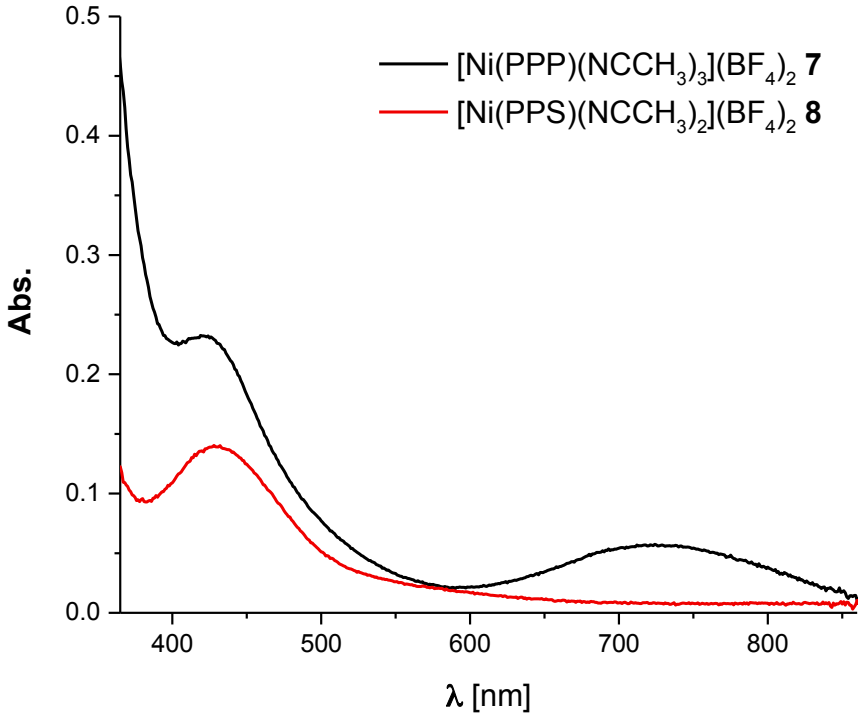

Figure S1. UV/vis spectra of Ni-complexes **7** and **8**.

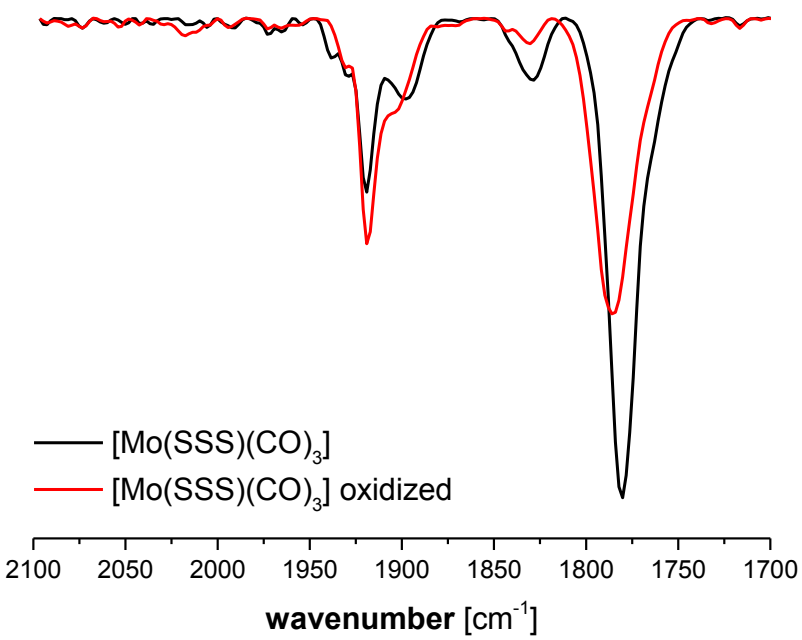

Figure S2. IR spectrum of compound **11** in tetrahydrofuran (black) and SEC-IR of **11** afterward oxidation (red).

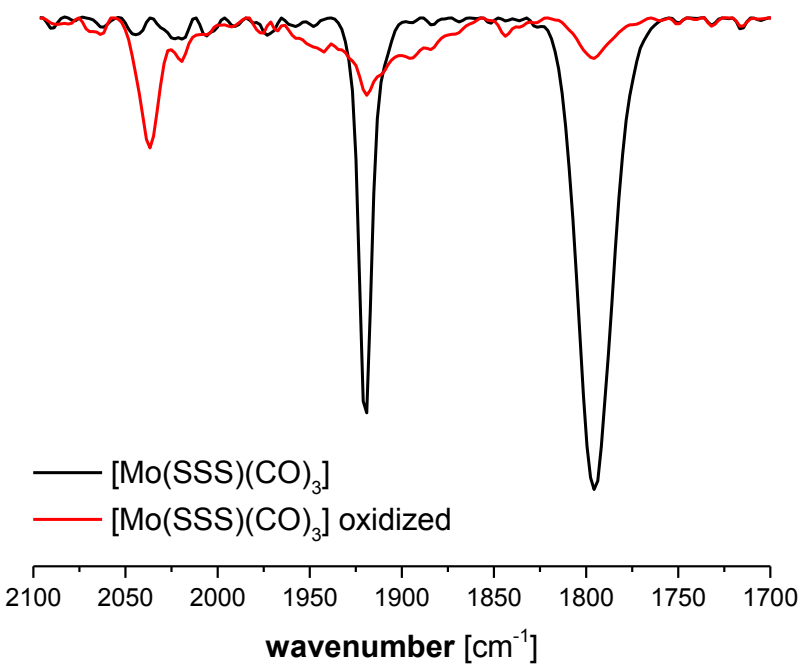

Figure S3. IR spectrum of compound **11** in acetonitrile (black) and SEC-IR of **11** afterward oxidation (red).

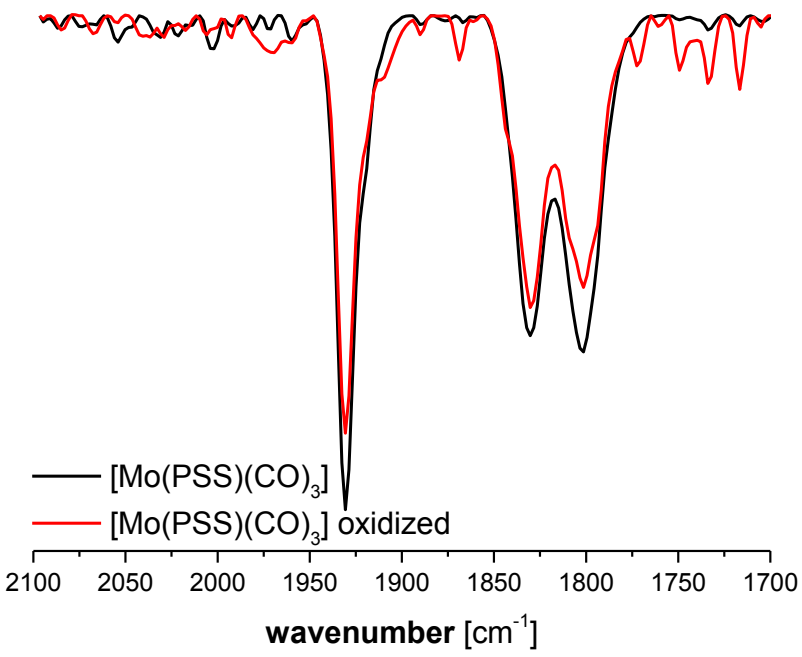

Figure S4. IR spectrum of compound **12** in acetonitrile (black) and SEC-IR of **12** afterward oxidation (red).

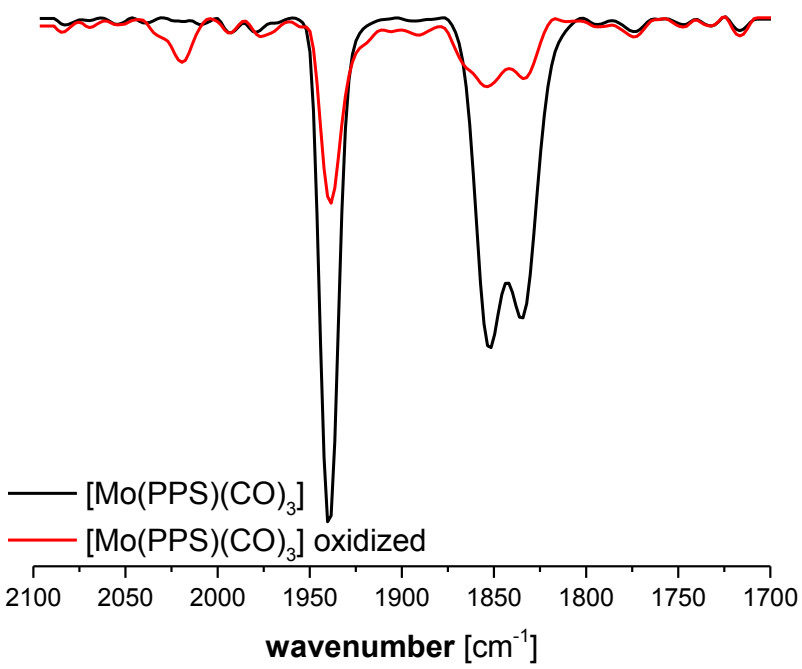

Figure S5. IR spectrum of compound **13** in tetrahydrofuran (black) and SEC-IR of **13** afterward oxidation (red).

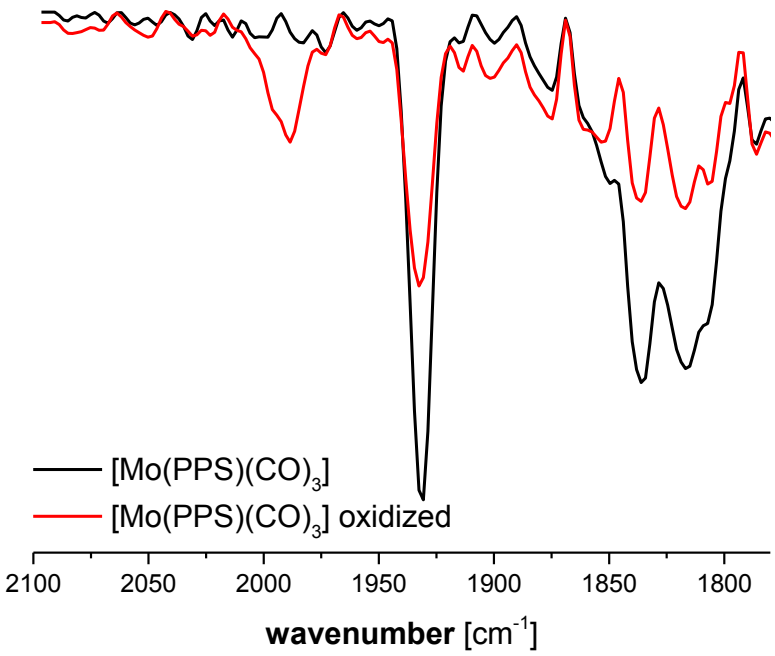

Figure S6. IR spectrum of compound **13** in acetonitrile (black) and SEC-IR of **13** afterward oxidation (red).

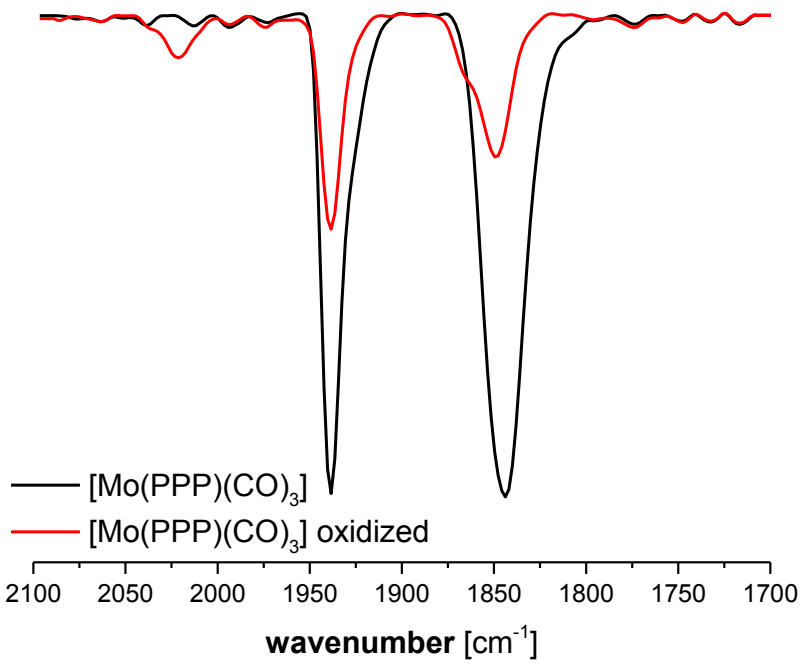

Figure S7. IR spectrum of compound **14** in tetrahydrofuran (black) and SEC-IR of **14** afterward oxidation (red).

Table S1. Overview of the calculated Gibbs free energies [Hartree], BP86 functional, Def2-tzvp basis set, of $[Mo^0(S_xP_{3-x})(CO)_y]$ (x = 0,1,2,3; y = 2,3; *vacuo*). Compounds **11** – **14** in different configurations.

	11	**12**	**13**	**14**
κ^3	-2626.95096	-2801.82129	-2976.63085	-3151.4285
κ^2S,S	-2626.99085	-2801.78686	-	-
κ^2S,S-MeCN	-2626.99236	-2801.79127	-	-
κ^2P,S	-	-2801.67451	-2976.5836	-
κ^2P,S-MeCN	-	-2801.66858	-2976.47256	-
κ^2P,P	-	-	-2976.61043	-3151.305
κ^2P,P-MeCN	-	-	-2976.60784	-3151.4108
κ^3-$(CO)_2$	-2626.94259	-2801.75228	n.d.	-3151.3779

Table S2. Overview of the calculated Gibbs free energies [Hartree], BP86 functional, Def2-tzvp basis set, of $[Mo^I(S_xP_{3-x})(CO)_y]$ (x = 0,1,2,3; y = 2,3; *vacuo*). The oxidized versions of compounds **11** – **14** in different configurations.

	11^+	**12^+**	**13^+**	**14^+**
κ^3	-2493.957427	-2668.773536	-2843.583961	-3018.389765
κ^2S,S-MeCN	-2493.963961	-2668.752420	-	-
κ^2P,S-MeCN	-	-2668.764135	-2843.557868	-
κ^2P,P-MeCN	-	-	-2843.570569	-3018.369293
κ^3-$(CO)_2$	-2493.949821	-2668.760840	-2843.571938	-3018.373680

Table S3. General overview of binding modes of the complexes in MeCN and upon oxidation supported by DFT calculations. The terms slow and fast correspond to the time scale of the spectroelectrochemical measurements, which was the same for all complexes.

	Mo^0-MeCN	**Mo^I-MeCN**
11	κ^2	$\kappa^2 \rightarrow$ fast degradation
12	κ^3	κ^3, $\kappa^2 \rightarrow$ slow degradation
13	κ^3	κ^3, $\kappa^2 \rightarrow$ slow degradation
14	κ^3	n.d.

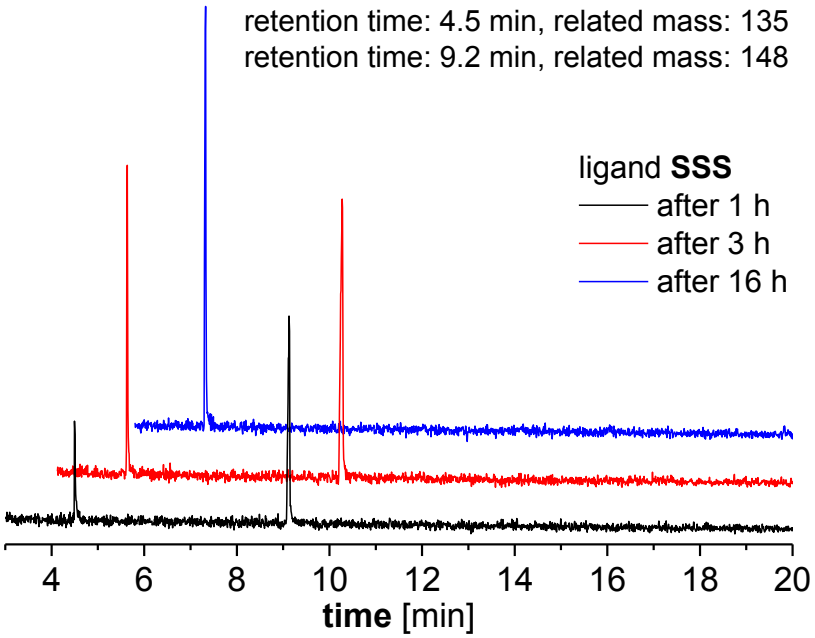

Figure S8. Gas chromatogram for the reduction of amides, catalyzed by $Fe_3(CO)_{12}$ (2 mol%) and ligand **SSS** (2 mol%) after 1 h (black), 3 h (red) and 16 h (blue).

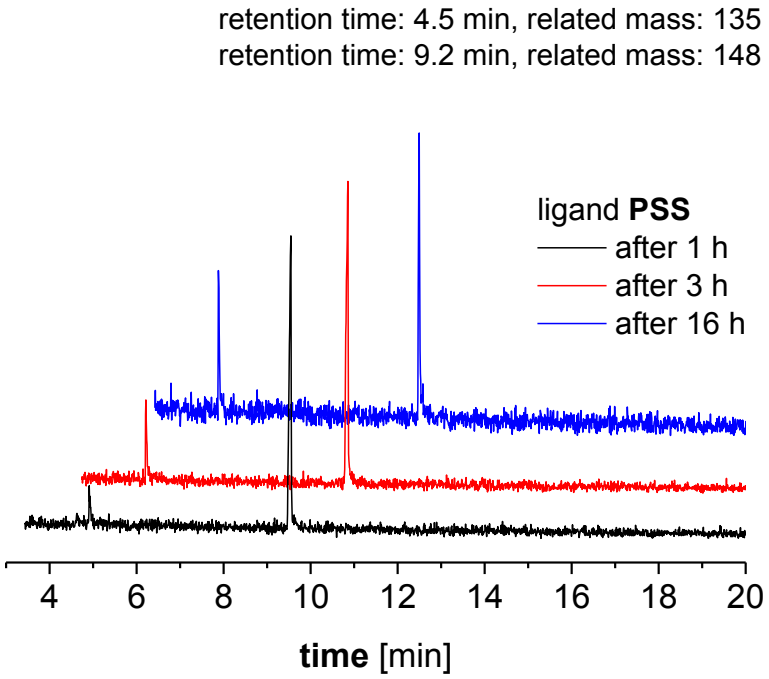

Figure S9. Gas chromatogram for the reduction of amides, catalyzed by $Fe_3(CO)_{12}$ (2 mol%) and ligand **PSS** (2 mol%) after 1 h (black), 3 h (red) and 16 h (blue).

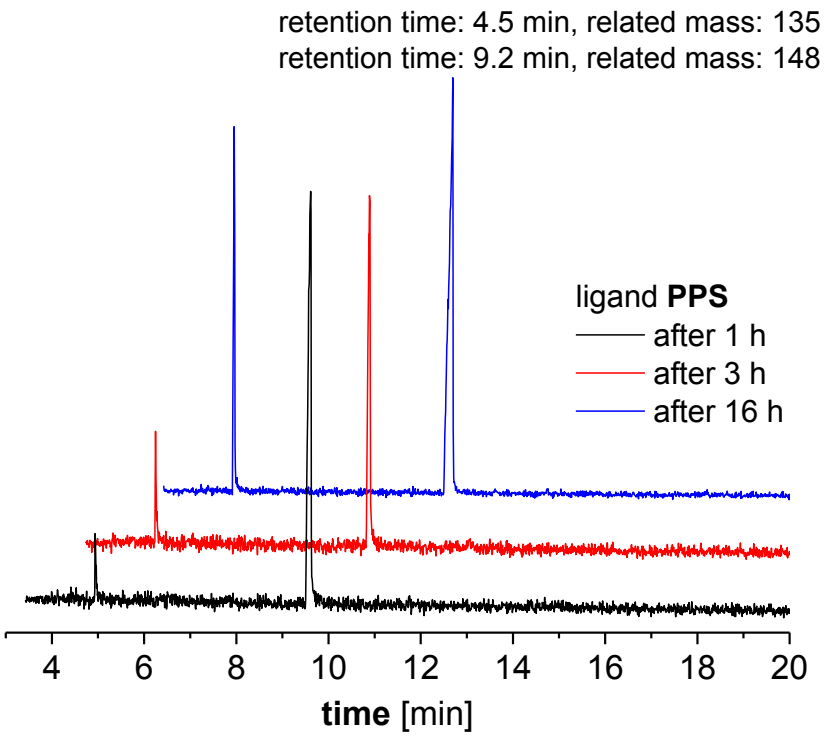

Figure S10. Gas chromatogram for the reduction of amides, catalyzed by $Fe_3(CO)_{12}$ (2 mol%) and ligand **PPS** (2 mol%) after 1 h (black), 3 h (red) and 16 h (blue).

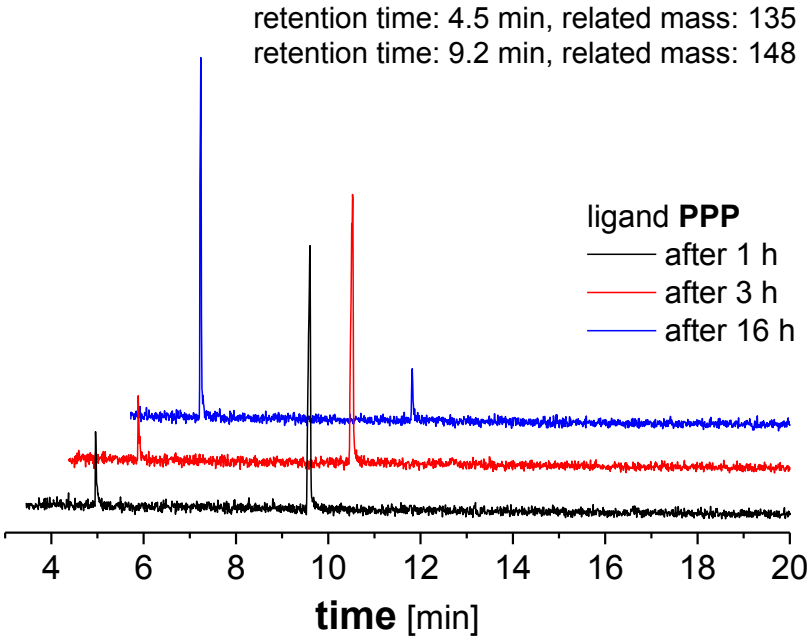

Figure S11. Gas chromatogram for the reduction of amides, catalyzed by $Fe_3(CO)_{12}$ (2 mol%) and ligand **PPP** (2 mol%) after 1 h (black), 3 h (red) and 16 h (blue).

Table S4. Crystal Data and Refinement Details for the Crystal Structure Analysis of Compound **8**, **9** and **11 - 14**.

	8	**9**	**11**
Empirical formula	$C_{41}H_{43}B_2F_8N_3NiP_2S$	$C_{35}H_{34}Cl_2FeP_2S$	$C_{56}H_{56}Mo_2O_7S_6$
Formula weight	904.11	675.37	1225.24
Temperature/K	106.7(2)	293	100.00(10)
Crystal system	orthorhombic	monoclinic	triclinic
Space group	*Pca*2$_1$	*Cc*	*P*-1
a/Å	25.31933(15)	18.571(14)	9.9426(4)
b/Å	9.23175(6)	17.955(14)	10.0256(4)
c/Å	17.87030(15)	9.942(11)	15.2661(6)
α/°	90	90	73.959(3)
β/°	90	90.48(2)	73.188(3)
γ/°	90	90	74.464(3)
Volume/Å^3	4177.04(5)	3315(5)	1370.46(10)
Z	4	4	1
ρ_{calc}/g·cm^{-3}	1.438	1.353	1.485
μ/mm^{-1}	2.470	0.799	6.291
F(000)	1864.0	1400.0	628.0
Crytsal size/mm^3	0.301x0.108x0.052	0.28x0.22x0.17	0.34x0.13x0.09
2θ range for data collection/°	6.983 to 148.201	3.156 to 49.994	9.376 to 152.796
Reflections collected	19119	14024	14246
Independent reflections	7554 [R_{int} = 0.0192]	5818 [R_{int} = 0.0434]	5540 [R_{int} = 0.0229]
Data/restraints/parameters	7554/1/554	5818/2/372	5540/0/311
[a]Goodness-of-fit on F^2	1.046	1.097	1.010
[b,c]Final R indexes [I≥2σ (I)]	R_1 = 0.0235, wR_2 = 0.0625	R_1 = 0.0483, wR_2 = 0.1233	R_1 = 0.0353, wR_2 = 0.0901
Final R indexes [all data]	R_1 = 0.0236, wR_2 = 0.0626	R_1 = 0.0555, wR_2 = 0.1414	R_1 = 0.0399, wR_2 = 0.0922
Largest diff. peak/hole/e·Å^{-3}	0.51/-0.26	1.62/-0.45	1.50/-1.08
CCDC reference	1545160	1545161	1545164

[a] $S = \{\sum[w(F_o^2-F_c^2)^2]/(n-p)\}^{0.5}$; n = no. of reflections; p = no. of parameters. [b] $R_1 = \sum||F_0|-|F_c||/\sum|F_0|$. [c] $wR_2 = \{\sum[w(F_o^2-F_c^2)^2]/\sum[w(F_o^2)^2]\}^{0.5}$.

	12	13	14
Empirical formula	$C_{32}H_{29}MoO_3PS_2$	$C_{42}H_{42}MoO_4P_2S$	$C_{44}H_{39}MoO_3P_3$
Formula weight	652.58	800.69	804.60
Temperature/K	170(2)	120(2)	170
Crystal system	monoclinic	monoclinic	trigonal
Space group	$P2_1/n$	$P2_1/n$	$R3$
a/Å	10.9008(6)	10.2574(7)	17.9235(14)
b/Å	16.6383(11)	17.4761(9)	17.9235(14)
c/Å	15.8862(9)	21.2556(15)	10.2589(9)
α/°	90	90	90
β/°	97.751(6)	100.417(7)	90
γ/°	90	90	120
Volume/Å^3	2855.0(3)	3747.5(4)	2854.2(5)
Z	4	4	3
ρ_{calc}/g·cm^{-3}	1.518	1.419	1.404
μ/mm^{-1}	0.695	4.520	0.511
F(000)	1336.0	1856.0	1242.0
Crystal size/mm^3	0.19x0.11x0.06	0.291x0.081x0.064	0.34x0.20x0.14
2θ range for data collection/°	5.9796 to 51.3618	6.592 to 154.29	6.582 to 73.16
Reflections collected	41654	37465	17979
Independent reflections	5407 [R(int) = 0.0965]	7773 [R(int) = 0.1243]	4527 [R(int) = 0.1558]
Data/restraints/parameters	5407/0/353	7773/0/452	4527/118/151
[a]Goodness-of-fit on F^2	1.008	1.037	1.065
[b,c]Final R indexes [I≥2σ (I)]	R_1 = 0.0452, wR_2 = 0.0762	R_1 = 0.0711, wR_2 = 0.1810	R_1 = 0.0938, wR_2 = 0.2094
Final R indexes [all data]	R_1 = 0.0719, wR_2 = 0.0868	R_1 = 0.1015, wR_2 = 0.2124	R_1 = 0.1216, wR_2 = 0.2400
Largest diff. peak/hole/e·Å^{-3}	0.71/-0.81	1.68/-0.78	4.01/-1.70
CCDC reference	1545163	1545162	1545379

[a] $S = \{\sum[w(F_o^2-F_c^2)^2]/(n-p)\}^{0.5}$; n = no. of reflections; p = no. of parameters. [b] $R_1 = \sum||F_0|-|F_c||/\sum|F_0|$. [c] $wR_2 = \{\sum[w(F_o^2-F_c^2)^2]/\sum[w(F_o^2)^2]\}^{0.5}$.

References

[1] Rigaku/MSC, *CrystalClear and CrystalStructure*, Rigaku/MSC Inc., The Woodlands, Texas, USA, **2006**.

[2] L. J. Farrugia, *J. Appl. Crystallogr.* **2012**, *45*, 849–854.

[3] A. L. Spek, *J. Appl. Crystallogr.* **2003**, *36*, 7–13.

[4] A. L. Spek, *Acta Crystallogr. Sect. D* **2009**, *65*, 148–155.

[5] G. M. Sheldrick, *Acta Crystallogr. Sect. A* **2008**, *64*, 112–122.

[6] O. V. Dolomanov, L. J. Bourhis, R. J. Gildea, J. A. K. Howard, H. Puschmann, *J. Appl. Crystallogr.* **2009**, *42*, 339–341.

[7] C. B. Hübschle, G. M. Sheldrick, B. Dittrich, *J. Appl. Crystallogr.* **2011**, *44*, 1281–1284.

[8] F. Neese, *Wiley Interdiscip. Rev. Comput. Mol. Sci.* **2012**, *2*, 73–78.

[9] A. D. Becke, *Phys. Rev. A* **1988**, *38*, 3098–3100.

[10] D. A. Pantazis, X.-Y. Chen, C. R. Landis, F. Neese, *J. Chem. Theory Comput.* **2008**, *4*, 908–919.

[11] E. van Lenthe, J. G. Snijders, E. J. Baerends, *J. Chem. Phys.* **1996**, *105*, 6505–6516.

[12] E. van Lenthe, A. van der Avoird, P. E. S. Wormer, *J. Chem. Phys.* **1998**, *108*, 4783–4796.